Tracking a defined route for O_2 migration in a dioxygen-activating diiron enzyme

Woon Ju Song[a], Grant Gucinski[b], Matthew H. Sazinsky[b], and Stephen J. Lippard[a,1]

[a]Department of Chemistry, Massachusetts Institute of Technology, Cambridge, MA 02139; and [b]Department of Chemistry, Pomona College, Claremont, CA 91711

Edited by J. Martin Bollinger, Pennsylvania State University, University Park, PA, and accepted by the Editorial Board July 19, 2011 (received for review April 27, 2011)

For numerous enzymes reactive toward small gaseous compounds, growing evidence indicates that these substrates diffuse into active site pockets through defined pathways in the protein matrix. Toluene/*o*-xylene monooxygenase hydroxylase is a dioxygen-activating enzyme. Structural analysis suggests two possible pathways for dioxygen access through the α-subunit to the diiron center: a channel or a series of hydrophobic cavities. To distinguish which is utilized as the O_2 migration pathway, the dimensions of the cavities and the channel were independently varied by site-directed mutagenesis and confirmed by X-ray crystallography. The rate constants for dioxygen access to the diiron center were derived from the formation rates of a peroxodiiron(III) intermediate, generated upon treatment of the diiron(II) enzyme with O_2. This reaction depends on the concentration of dioxygen to the first order. Altering the dimensions of the cavities, but not the channel, changed the rate of dioxygen reactivity with the enzyme. These results strongly suggest that voids comprising the cavities in toluene/*o*-xylene monooxygenase hydroxylase are not artifacts of protein packing/folding, but rather programmed routes for dioxygen migration through the protein matrix. Because the cavities are not fully connected into the diiron active center in the enzyme resting state, conformational changes will be required to facilitate dioxygen access to the diiron center. We propose that such temporary opening and closing of the cavities may occur in all bacterial multicomponent monooxygenases to control O_2 consumption for efficient catalysis. Our findings suggest that other gas-utilizing enzymes may employ similar structural features to effect substrate passage through a protein matrix.

dioxygen transfer | metalloenzyme | stopped-flow kinetics | diiron monooxygenase

A large number of metalloenzymes utilize dioxygen as a substrate. Understanding the process by which O_2 gains access to the active sites in these proteins has been a great challenge. Common substrates in biological systems, such as protons and electrons, require specific environments to facilitate translocation (1–4). By contrast, gaseous substrates like dioxygen may quickly diffuse through a protein matrix without direct assistance of specific local residues. Several enzymes that utilize gas molecules, such as O_2 (5, 6), H_2 (6, 7), or CO (8), as substrates have been investigated to understand how these small substances traverse the protein to reach their active sites. Most studies depended primarily on X-ray crystallography combined with Xe pressurization experiments to determine hydrophobic voids within the protein architecture that can be utilized to delineate substrate passage. The strong electron density and similar van der Waals diameter of xenon (4.3 Å) compared to that of O_2 (3.0–4.3 Å) renders it a useful surrogate for visualizing possible dioxygen routes within proteins by X-ray crystal structure analysis (5, 7). Because small gaseous molecules bind in a nonselective manner to the hydrophobic cavities in a protein, however, further evidence is required to elucidate the actual O_2 migration pathway.

Bacterial multicomponent monooxygenases (BMMs) utilize dioxygen, protons, and electrons as cosubstrates for hydrocarbon oxidation. Dioxygen activation, inter- and intraprotein electron transfer, proton translocation, and C-H oxidation occur through orchestrated motions of three or four components, a hydroxylase, regulatory protein, reductase, and/or Rieske protein (9, 10), such that the kinetics of substrate consumption and product formation are finely tuned. BMMs have been extensively investigated over the past two decades (11, 12). Complexity from multiple and concurrent reactions involving several component proteins, however, has impeded the elucidation of important chemical steps during catalysis, including dioxygen migration to the active site.

The first X-ray structure of a BMM, soluble methane monooxygenase hydroxylase (sMMOH) (13), revealed the diiron active center to lie adjacent to a hydrophobic pocket, buried approximately 12 Å beneath the protein surface. As a first step in approximating the dioxygen transfer pathway in sMMOH, a structure using crystals pressurized with xenon gas was obtained (14). The Xe atoms localize in a few isolated hydrophobic sites in the α-subunits of the enzyme, hereafter referred to as cavities. Similar results were obtained for another BMM, phenol hydroxylase hydroxylase (PHH), suggesting that the conserved cavities possibly function as a universal dioxygen transfer pathway (15). This working model, derived only from resting-state enzyme structures, neglects dynamic events that might occur during catalysis. Moreover, the discovery of an extended channel through the α-subunits in toluene/*o*-xylene monooxygenase hydroxylase (ToMOH) provided an alternative architecture of potential relevance for dioxygen transfer (16). This finding raised the question, for the BMM family, how does dioxygen access the active sites and is there a conserved pathway?

To address this question, a method other than structural characterization was required. For ToMOH variants, measuring catalytic efficiency, k_{cat}/K_M (O_2), was not feasible because the steady-state activity of BMMs, as measured by the formation rate of oxidized hydrocarbon product, is independent of dioxygen concentration and therefore not reflective of the dioxygen migration step (15). Molecular dynamics simulations may not be easily applicable to BMMs because significant structural changes are expected to occur via component interactions during catalysis. Instead, we directly measured the dependence of the oxygenation rate of the diiron center in the enzyme on the O_2 concentration under pre-steady-state conditions and compared the results for

Author contributions: W.J.S. and S.J.L. designed research; W.J.S., G.G., and M.H.S. performed research; W.J.S., G.G., M.H.S., and S.J.L. analyzed data; and W.J.S. and S.J.L. wrote the paper.

The authors declare no conflict of interest.

This article is a PNAS Direct Submission. J.M.B. is a guest editor invited by the Editorial Board.

Data deposition: The atomic coordinates and structure factors have been deposited in the Protein Data Bank, www.pdb.org (PDB ID codes 3RNC, 3RNA, 3RNG, 3RNB, 3RNF, 3RN9, 3RNE).

[1]To whom correspondence should be addressed. E-mail: lippard@mit.edu.

This article contains supporting information online at www.pnas.org/lookup/suppl/doi:10.1073/pnas.1106514108/-/DCSupplemental.

several variants in which the volume occupied by the side chain of different amino acids along putative O_2 pathways was altered by site-directed mutagenesis. This approach was possible because an oxygenated intermediate (first termed $T201S_{peroxo}$ and later $T201_{peroxo}$, $\lambda_{max} = ca.\ 675$ nm) was previously identified in a T201S ToMOH variant during dioxygen activation by reduced ToMOH in the presence of its cognate regulatory protein, ToMOD, and formed at rates that were linearly dependent on the concentration of O_2 (17). This result indicated that O_2 access to the diiron site is a rate-limiting step in $T201_{peroxo}$ formation under pre-steady-state conditions. Thus, the $T201_{peroxo}$ formation rate can reveal the rate of dioxygen migration/binding to the diiron active site, which has never been explored in any diiron-containing enzyme. Because the T201S variant is active in steady-state catalysis, preserving the single-turnover yields and regiospecificity of the native enzyme (18), the results of this study are physiologically relevant to the dioxygen transfer pathway in the native ToMO system. Although sMMOH is the more thoroughly investigated BMM, there are two experimental limitations to the application of the same methodology for this enzyme. First, the dioxygen access or binding step has never been directly observed. Upon the reaction of reduced sMMOH with dioxygen in the presence of its regulatory protein, the first oxygenated species to appear does so at rates much slower than the decay rate of the reduced diiron centers, indicating that O_2 consumption is coupled with, or preceded by, slower step (s), possibly structural reorganization or formation of uncharacterized intervening species (19, 20). In addition, a recombinant expression system to produce sMMOH variants in sufficient quantities for detailed kinetic studies has never been achieved. Toluene monooxygenases including ToMOH, however, can be expressed in *Escherichia coli*, thus facilitating site-directed mutagenesis studies (21, 22).

Based on the X-ray structures of ToMOH (Fig. 1*A*), nine residues from among those identified as plausible candidates along the dioxygen transfer pathway were selected for mutagenesis. Design and selection were also aided by the structure of an analogous protein, toluene 4-monooxygenase hydroxylase, in complex with its regulatory protein (T4moH–T4moD or T4moHD) (23) (Fig. 1*B*); a similar structure is not yet available for the ToMO system. The variants were designed primarily based on size rather than hydrophobicity with the assumption that steric bulk and the attendant alterations in the volume of the pathways are most critical for controlling O_2 access (24). Two mutations, however, were designed to probe hydrophobicity as well as the size of the amino acids because a polar residue may contribute to the slower rate of dioxygen transfer (25). In the experiments described here, a T201S mutation was introduced to provide a sensor, in the form of an optical transition at 675 nm (17), to detect dioxygen arrival at the diiron sites via formation of the $T201_{peroxo}$ intermediate. Double or triple variants were prepared and crystallographically characterized to evaluate whether or not the additional mutation would modify the dimensions of various hydrophobic sites along a putative pathway chosen for interrogation. Finally, $T201_{peroxo}$ formation rates were individually measured from the reaction of the reduced ToMOH variants and dioxygen in the presence of ToMOD to evaluate whether the steric alterations along the potential O_2-migration pathways would result in increases or decreases in the dioxygen transfer rates.

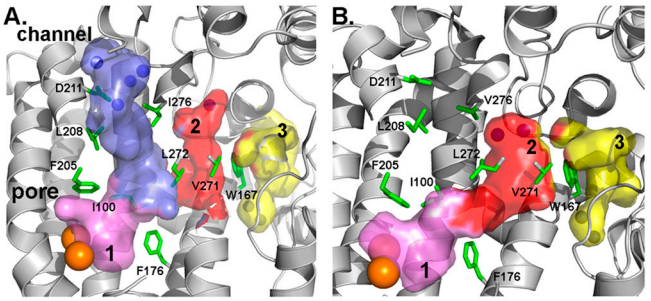

Fig. 1. Cartoon representation of the cavities and channel. (*A*) ToMOH (2INC). (*B*) T4moH–T4moD complex (3I5J). Residues I100, W167, F176, F205, L208, D211, V271, L272, and I276 or V276 are depicted as green sticks. Water occupying cavities and channel are represented as blue spheres. The diiron center is denoted by orange spheres. A molecule of PEG 400, occasionally observed in the ToMOH channel (blue surfaces), is not depicted.

Results and Discussion

Structural Analysis of ToMOH and Design of Mutants. An X-ray crystal structure of ToMOH revealed three potential access routes leading from the protein exterior to the diiron active sites as putative dioxygen transfer pathways (15, 16). They are a series of adjacent cavities, a pore, and a channel. Similar features occur in the structure of T4moH (23).

The first route comprises three adjacent hydrophobic cavities 1, 2, and 3, numbered according to their increasing distance from the diiron active site (Fig. 1*A*). They are observed in all structurally characterized BMMs. In previous X-ray studies conducted with crystals of BMM hydroxylases exposed to Xe under pressure, this inert gas was readily observed in the cavities (14, 15). This finding suggested that the cavities might serve as access routes for O_2 and/or small hydrophobic molecules such as CH_4 to the active site.

The pore is the smallest and shortest pathway from bulk solvent to the active sites. It is conserved in some BMMs, with a size and shape that varies depending on the enzyme. Structural studies of PHH and T4moH in complex with their respective regulatory proteins revealed that the latter bind to the hydroxylase where the pore region exits the protein surface approximately 12 Å above the diiron center (23, 26). Because of this interaction, the pore is no longer exposed to solvent and therefore less likely to provide a route for dioxygen access; the regulatory proteins are required for dioxygen activation. Based on these observations, we excluded the possibility that the pore is involved in dioxygen transfer.

The second available route for dioxygen migration is a long hydrophobic channel found only in toluene monooxygenases including ToMOH and T4moH that measures 6–10 Å in width and 30–35 Å in length, more than sufficient to accommodate dioxygen passage (16, 23). The channel is connected to the diiron active site, overlapping with cavities 1 and 2 at the entryway (Fig. 1*A*). It is therefore a plausible path for dioxygen as well as arene substrate migration, for which it was originally proposed. Extensive structural changes occur in the channel upon binding of the regulatory protein (T4moD) to T4moH (T4moHD, Fig. 1*B*), however, altering the conformations of amino acid side chains and effectively closing it off from the protein exterior (23). The structures of T4moH and T4moHD suggest that the channel will transiently open and close during catalysis. Given that the rate of dioxygen migration must be fast enough to access even a transiently accessible pathway, we considered both the cavities and the channel as candidates for O_2 access to the diiron center.

To evaluate the dioxygen transfer pathway in ToMOH, we selectively mutated six residues that form the cavities, I100, W167, F176, F205, V271, and L272, and three that line the channel, L208, D211, and I276 (Fig. 1*A*). Each residue was altered to adjust the dimensions in its vicinity. As described above, T201 was also mutated to T201S in order to provide a convenient optical signal, arising from $T201_{peroxo}$ formation, by which to monitor the dioxygen transfer rate constants under pre-steady-state conditions.

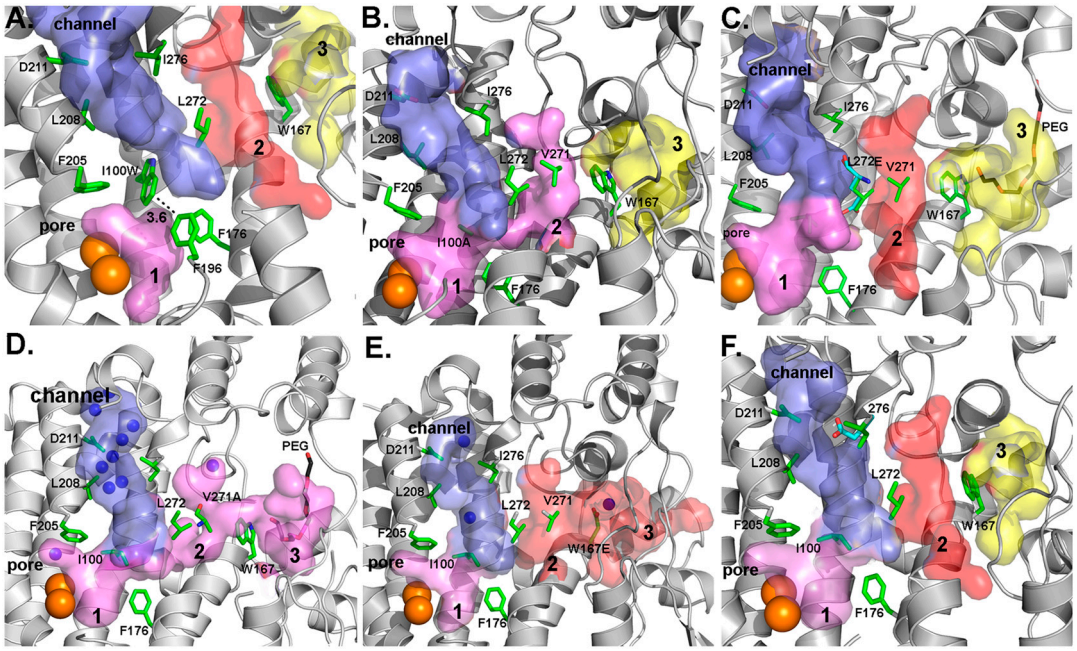

Fig. 2. Structural comparison of ToMOH variants. Structures were represented in the same manner as Fig. 1. (*A*) T201S/I100W, (*B*) T201S/I100A, (*C*) T201S/L272E, (*D*) T201S/V271A (i) T201S/W167E, (*F*) T201S/I276E. In *C* and *F*, side chains of L272 and I276 residues in the wild type in green were overlaid on the variants in cyan for comparison.

Fe Content and Activity Measurements. To assure that the mutations did not greatly perturb the global folding, component interactions, or active site structure of the enzyme system, the iron content and steady-state activity for phenol oxidation were measured. The variants were prepared and characterized as previously described (17). All 13 variants contained 3–4 iron atoms per protein dimer, similar to the content of the wild-type enzyme (*SI Appendix*, Table S2). Steady-state activities for phenol oxidation, measured as described previously (27), are listed in *SI Appendix*, Table S2 (21, 27). Results for the T201S/F176A, T201S/V271A, T201S/L272A, and T201S/I276E variants are comparable to those of the wild-type enzyme and T201S variant. The activities of T201S/I100A, T201S/W167E, T201S/F205A, and T201S/L272E were diminished, but only by approximately 3–10-fold relative to that of the wild-type enzyme. These results suggest that some chemical step(s) during steady-state catalysis are slightly perturbed, but confirm that all of the enzymes are still active and that the mutations do not greatly perturb the chemical properties of the diiron centers, such as the redox potential and their intrinsic O_2 affinity in the reduced state. For the substitution of a few residues, specifically I100, F176, or F205 with tryptophan, phenol oxidation activity was lost, probably because the newly supplied tryptophan residue serves as an internal substrate without affecting dioxygen activation at the diiron center, as previously observed (28). Formation of the one-electron oxidized product, a tryptophan-radical species, was monitored at 500 nm under pre-steady-state conditions, confirming that these variants are still able to activate dioxygen. The T201S/L208W and T201S/L208W/D211W variants were unable to oxidize phenol. We did not obtain optical spectroscopic evidence for tryptophan oxidation in these mutants, possibly because they are located at a distance too far from the diiron center. The inability of the T201S/L208W and T201S/L208W/D211W variants to function as external or internal arene oxidation catalysts may be a consequence of their inability to achieve the necessary conformational changes required for O_2 activation, rendering them unsuitable for the current purposes. Accordingly, these variants were not further pursued.

Structural and Kinetic Studies of ToMOH Variants. Structural alterations arising from each of the amino acid substitutions were evaluated by X-ray crystallography. Seven variants were prepared and structurally characterized, namely, T201S/I100W, T201S/F176W, T201S/I100A, T201S/L272E, T201S/V271A, T201S/W167E, and T201S/I276E (Fig. 2 and *SI Appendix*, Fig. S3 and Table S3). None caused misfolding or global structural changes in the protein, only local alterations near the modified side chain. Rates of dioxygen passage to the diiron active sites were measured by the following procedure. Reduced ToMOH variants in complex with ToMOD ($ToMOH_{red}D$) were allowed to react with O_2-dissolved buffer in the stopped-flow spectrophotometer at 4 °C. Time-dependent absorption changes arising from the formation and decay of $T201_{peroxo}$ were monitored at 675 nm. The traces were very well fit to a function derived from two consecutive irreversible processes, reduced ToMOH → $T201_{peroxo}$ → oxidized ToMOH, from which formation rate constants (k_{form}) could be derived. In the T201S single variant, k_{form} is linearly dependent on O_2 concentration, yielding the second-order formation rate constant (k_2) of 0.22 ± 0.01 $\mu M^{-1} s^{-1}$, as reported previously (17) (*SI Appendix*, Fig. S2*A*). This value is significantly less than that expected for a purely diffusion-controlled encounter (*ca.* 10^9 $M^{-1} s^{-1}$), implying that O_2 migration through the protein slows down access to the active site diiron center and is probably coupled to structural fluctuations.

Tracking O_2 Entrance to Cavity 1. The I100 residue is located at the entry position to cavity 1 (Fig. 1). Based on the sequence and structural alignments, I100 in ToMOH was previously proposed to be the analog of L110 in sMMOH, gating access to the active site (29). Two different conformations at L110 occur in two crystal forms of sMMOH, suggesting that L110 may shift its position to control the opening of cavity 1 during catalysis. Analogously, different conformations at I100 occur upon binding of the regulatory protein in the T4moHD structure (*SI Appendix*, Fig. S1*A*), with the binding of the regulatory protein causing the side chain to swing out, opening access to the diiron center.

Conversion of residue I100 to tryptophan in the T201S/I100W variant partially occludes active site entry from cavity 1, the indole ring stacking on F196 at a nearly van der Waals distance of

3.6 Å (Fig. 2*A*). The closest C···C distance of I100 to F196 in the wild-type enzyme is 5.9 Å. The structural changes, however, do not greatly perturb the dioxygen activation at the diiron center as demonstrated in the spectroscopic studies of the I100W single variant (30). The dioxygen diffusion rate should therefore be diminished if I100 were on the O_2 migration pathway. Pre-steady-state studies of the reaction of a T201S/I100W ToMOH$_{red}$D preformed complex with O_2 revealed that k_{form} is linearly dependent on the O_2 concentration, but has a rate constant approximately threefold less than that of the T201S variant (Table 1 and *SI Appendix*, Fig. S2*B*). The data indicate that the I100W mutation retards dioxygen passage, consistent with cavity 1 being on the dioxygen transfer pathway. The decay rate of the T201$_{peroxo}$ intermediate in the T201S/I100W variant was accelerated relative to the value for the T201S variant because the indole ring at I100W served as an internal substrate for T201$_{peroxo}$, as described previously (31).

In addition to the I100W variant, T201S/F176W and T201S/F205W mutated proteins were investigated to probe further the putative role of cavity 1 in facilitating O_2 access to the active site (Fig. 1 and *SI Appendix*, Fig. S3). Structural and kinetic alterations as a result of the F176W and F205W mutations were expected to be similar to those observed for I100W, limiting O_2 access to the diiron center. Reaction of neither T201S/F176W nor T201S/F205W ToMOH$_{red}$D with dioxygen, however, produced the T201$_{peroxo}$ optical spectrum. Instead, spectral changes at 500 nm, a characteristic feature of a tryptophan-radical species, were monitored as observed in the T201S/I100W mutant. This observation suggests that these variants presumably perform dioxygen activation and generate T201$_{peroxo}$, similar to the T201S variant, but the proximity of F176W and F205W to the diiron center caused the peroxo intermediate to react more rapidly with the indole side chain and to decay without accumulation.

The I100A mutation brings about a different structural effect at I100 compared to the I100W, F176W, and F205W variations, enlarging the entrance to cavity 1, as revealed by an X-ray crystal structure analysis of T201S/I100A (Fig. 2*B*). In this variant, the shortest C···C distance increases from 5.9 to 8.1 Å. As a result, cavity 1 becomes large enough to be fully connected to cavity 2. Although crystal structures of the F176A and F205A variants were not determined, PyMOL (32) models suggested that the mutations increase the size of cavity 1. The abilities of the T201S/I100A, T201S/F176A, and T201S/F205A variants to activate dioxygen were individually monitored. None showed any evidence for a significant build up of the T201$_{peroxo}$, although they were still active for phenol oxidation under steady-state conditions. One possibility is that adventitious water/proton(s) become accessible through the larger cavity 1 in I100A, F176A, and F205A mutants, which might quench T201$_{peroxo}$, leading to the release of H_2O_2. Such autoxidation due to the opening of hydrophobic sites near the active site was previously observed for variants of myohemerythrin (33).

O_2 Passage Through Cavity 2. Residue L272 is located between cavities 1 and 2, close to the intersection with cavity 1 and the channel. The closest C···C distances between L272 and cavity 1 (F196) or channel (Q204) residues are 10.6 and 6.1 Å, respectively. Structures of T4moH in the absence and presence of T4moD reveal that the orientation of the L272 side chain can vary significantly, suggesting a leucine gate (*SI Appendix*, Fig. S1*A*) similar to that identified in sMMOH (29). A glutamate mutation at position 272 was chosen because its side chain can extend farther into the cavity than that of leucine, despite its slightly smaller total volume. Such a projection will diminish the local hydrophobicity and influence the rate of dioxygen migration through that region of the protein (25). These anticipated structural and polarity changes suggested that the T201$_{peroxo}$ formation rate would decrease if L272 were on the O_2 migration pathway. The ToMOH

Table 1. T201$_{peroxo}$ formation rates in ToMOH variants

Mutant	Second-order formation rate constant, s^{-1} μM^{-1}	Relative second-order formation rate constant to the T201S variant
T201S	0.21 ± 0.01	—
T201S/I100W	0.06 ± 0.01	0.29 ± 0.05
T201S/L272E	0.12 ± 0.04	0.57 ± 0.19
T201S/I276E	0.29 ± 0.08	1.38 ± 0.38
T201S/V271A	0.43 ± 0.05	2.05 ± 0.24
T201S/W167E	0.77 ± 0.11	3.67 ± 0.55

Second-order formation rate constants were obtained from pre-steady-state reaction between dioxygen and at least three independently prepared batches of the protein samples (*SI Appendix*, Fig. S2). Relative second-order formation rate constant is the rate constant normalized to that of the T201S variant, as described in the text.

L272E crystal structure confirmed that the mutation reduced the size of the protein interior at the point where cavity 1, cavity 2, and the channel merge (Fig. 2*C* and *SI Appendix*, Fig. S1*B*). As a consequence, the L272E and F196/Q204 residues are 6.1 and 5.9 Å apart, respectively. Reaction of the T201S/L272E variant of ToMOH$_{red}$D with O_2 generated T201$_{peroxo}$, but yielded a rate constant, approximately twofold less than the value of the T201S variant (Table 1 and *SI Appendix*, Fig. S2*C*). This result reveals that cavity 2 is a part of the dioxygen transfer pathway, in conjunction with cavity 1.

A T201S/L272A variant was prepared to gauge the effect of an enlarged cavity 2, because removal of the side chain at L272 makes cavity 2 significantly wider than the native and T201S enzymes. Dioxygen activation of the T201S/L272A, however, revealed no detectable formation of T201$_{peroxo}$, probably due to autoxidation as encountered in the T201S/I100A, T201S/F176A, and T201S/F205A mutants described above.

V271 is located in cavity 2. The side chain resides at the interface between cavity 2 and cavity 3 and possibly gates movement between the two cavities during catalysis. The V271A mutation enlarges cavity 2 and creates a direct path from cavity 1 to cavity 3 (Fig. 2*D*). During dioxygen activation in the T201S/V271A variant, formation of T201$_{peroxo}$ was observed, yielding a second-order formation rate constant of approximately twice that in T201S (Table 1 and *SI Appendix*, Fig. S2*D*). This result, in addition to the L272E mutation, therefore, indicates that cavity 2 is utilized in dioxygen transfer.

Cavity 3 Also Helps to Convey O_2 to the Active Site. The indole ring of residue W167 is located at the interface between cavities 2 and 3 (Fig. 1 and *SI Appendix*, Fig. S4). In the W167E variant, however, hydrogen-bonding interactions with T341 and E166 draw the glutamate side chain out of the interstitial space between cavities 2 and 3 (Fig. 2*E* and *SI Appendix*, Fig. S4). As a result, cavities 2 and 3 merge to form a single chamber, large enough for dioxygen to traverse. When dioxygen was allowed to react with the T201S/W167E variant of ToMOH$_{red}$D, the second-order formation rate constant was measured to be approximately threefold greater than that of the T201S variant (Table 1 and *SI Appendix*, Fig. S2*E*). The acceleration of dioxygen migration to the diiron center arising from this single mutation at W167 reveals that cavity 3 is also on the path of dioxygen transfer, allowing it to pass on to cavities 2 and 1 to the active site diiron center. It is worth noting that, in the crystal structures of T201S/L272E and T201S/V271A, a PEG 400 molecule was observed in cavity 3, which may delineate how O_2 gains access to this cavity from the protein surface (Fig. 2 and *SI Appendix*, Fig. S5).

The Channel Is Not a Primary Route of O_2 to the Active Site. Residues I276 and L208 are located at the narrowest part of the channel and lie opposite one another. The closet distance between two

carbon atoms involving these residues is 5.8 Å. Replacement of I276 with glutamate (I276E) lengthens the side chain and diminishes the size of the channel (Fig. 2*F*), the shortest distance between I276E and L208 atoms being 4.6 Å. The mutation, again, increases the hydrophilicity and, as a result, may retard the access of dioxygen if the channel were involved in O_2 transfer to the active site. Reaction of the T201S/I276E variant with dioxygen returned a second-order formation rate constant for $T201_{peroxo}$ that was unaltered from the value in the T201S variant (Table 1 and *SI Appendix*, Fig. S2*F*). This result strongly suggests that the channel is not a primary pathway for dioxygen delivery.

To highlight the kinetic effects on dioxygen transfer for the five mutants just discussed, we generated relative second-order $T201_{peroxo}$ formation rate constants ($k_{2,T201S/X}/k_{2,T201S}$) by dividing the individual rate constant in the double variants ($k_{2,T201S/X}$) by that for the T201S enzyme ($k_{2,T201S}$) (Table 1 and Fig. 3). Decreasing the size of the cavities in the I100W and L272E variants retards the dioxygen transfer rate constants, with $k_{2,T201S/X}/k_{2,T201S} < 1$. The opposite effect was encountered for V271A and W167E in the cavities, $k_{2,T201S/X}/k_{2,T201S}$ being > 1. In contrast, decreasing the channel volume by forming the I276E variant yielded $k_{2,T201S/X}/k_{2,T201S}$ of approximately 1. This combination of kinetic and structural information establishes that the three cavities, but not the channel, supply dioxygen to the active site of the enzyme.

The Need for Conformational Changes During Dioxygen Activation. The foregoing structural and kinetic studies demonstrate that cavities 1–3 are utilized for dioxygen transfer. In the resting-state structures of ToMOH (Fig. 1*A*) and T4moH, however, these cavities are not connected to one another. We therefore speculate that rapid conformational changes must occur during catalysis to form a connected trajectory for dioxygen access to the diiron active site. Simultaneously, the channel must close off to ensure selective delivery of O_2 through the cavities. The postulated protein fluctuations will probably occur on the microsecond timescale, based on the $T201_{peroxo}$ formation rates. Temporary opening/closing of hydrophobic sites is probably gated by the I100, L272, V271, and W167 residues as discussed above. Different orientations of these residues were in part observed in the T4moHD complex structure, where cavities 1 and 2 are connected, and the channel is sealed upon regulatory protein binding (23) (Fig. 1*B*). Therefore, component interactions between the hydroxylase and regulatory protein are critical for triggering breathing motions in the α-subunit of the hydroxylase and gate substrate access to the active site diiron center. This working hypothesis thus explains a previous report that introduction of the cognate regulatory protein, MMOB, to the sMMOH accelerates the rate of dioxygen consumption by approximately 1,000-fold (19). Although cavities 1 and 2 are connected as a consequence of the binding of the regulatory protein, further conformational changes are required to form a trajectory to the active site that includes cavity 3. Such a change might be induced by the presence of molecular oxygen itself, in a manner similar to that proposed previously for carbon monoxide in myglobin (34). Given that cavities appear to be a conserved feature of BMMs, they are most likely not simple packing defects but rather programmed units for O_2 migration in this family of proteins. It is also possible that such cavities are employed for small substrate access to the active site because halogenated alkanes were found to occupy a few cavities in sMMOH X-ray crystal structures of samples cocrystallized with these substances (14).

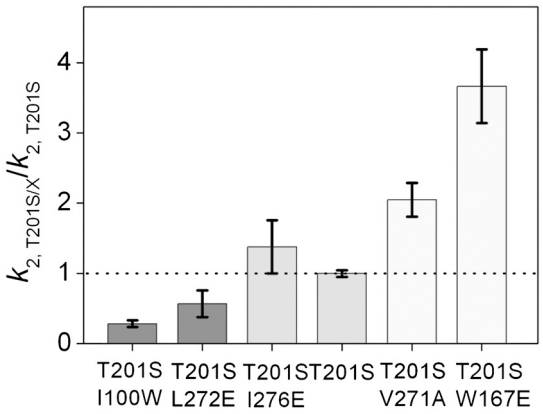

Fig. 3. Relative second-order formation rate constants of $T201_{peroxo}$ ($k_{2,T201S/X}/k_{2,T201S}$) in ToMOH variants. Depending on their relative second-order formation rates, columns were filled in dark gray, gray, and light gray for the values <1, ≈1, >1, respectively.

Because BMMs react with dioxygen even in the absence of hydrocarbon substrates, conformationally gated dioxygen migration is presumably a conserved strategy designed to control the choreographed consumption of multiple substrates in a timely manner. These simple but elegant protein motions physically increase and decrease the dimensions of the migration pathway, similar to the inhale/exhale motions of breathing. We speculate that the channel structure evolved for aromatic substrate access and/or product egress because it is found only in arene-oxidizing ToMOH and T4moH enzymes. We also conjecture that PHH, which catalyzes phenol oxidation, might have a channel for the same purpose. The absence of a well-defined aromatic substrate pathway in the only available X-ray structure of PHH (26) is now explicable because of the presence of the bound cognate regulatory protein, which we now know can close the channel, as observed in the T4moHD structure (23).

Concluding Remarks

Structural and kinetic studies of ToMOH variants have revealed that alterations in the size of a series of three cavities leading from the protein exterior to the active site measurably accelerate or decelerate dioxygen migration, as monitored by the formation of a peroxodiiron(III) intermediate upon reaction of the diiron (II) protein with dioxygen. Structural alterations of the channel by which aromatic substrates access the active site had no effect on the rate constant. These results are consistent with the working hypothesis that dioxygen access to the diiron center involves migration through the cavities, approximately 36–40 Å in overall distance. A previously reported structure of the related toluene monooxygenase hydroxylase, T4moH, supports the hypothesis that, in complex with its regulatory protein, the orientation of a few key residues can rearrange to form a specific pathway via the cavities for dioxygen transfer. Given that these cavities are conserved in all BMMs, the dioxygen migration path delineated here is likely to be universal in this family. Temporary protein breathing motions that open and close the cavities may regulate the consumption of small gaseous molecules in a variety of enzymes where the presence of all substrates is not required for reactivity.

Materials and Methods

General Considerations. Heterologous expression and purification of the four ToMO component proteins were carried out as described (18, 21). For site-directed mutagenesis, a pET22b(+)/touBEA T201S plasmid was used as the template as described previously (17). Primers used to generate the mutations are listed in *SI Appendix*, Table S1 and were obtained from Integrated DNA Technologies. Detailed procedures for iron assays (21) and specific activity assays (27) were described previously. These results are summarized in *SI Appendix*, Table S2. Extinction coefficients at 280 nm of the ToMOH variants were calculated based on the sequence (35).

Crystallization, Data Collection, Structure Determination, and Refinement. Seven ToMOH variants were crystallized by using previously published procedures (16, 30). X-ray diffraction data were collected at the Northeastern Collaborative Access Team beamline 24IDE or at Stanford Synchrotron Radia-

tion Lightsource beamline 12-2 and processed using either HKL2000 or iMosflm. Phasing of ToMOH data was accomplished by using MolRep and the 1.85-Å native ToMOH coordinates as described previously (36). Refinements and building were carried out by Refmac5 and Coot, respectively (*SI Appendix*, Table S3). The atomic coordinates have been deposited in the Protein Data Bank for Fig. 2 *A*–*G* and *SI Appendix*, Fig. S3, respectively.

Characterization of an Oxygenated Intermediate in ToMOH Variants by Optical Spectroscopy. Optical bands characteristic of the oxygenated intermediate in ToMOH T201S variants, $T201_{peroxo}$, were monitored by using a HiTech DX2 stopped-flow spectrophotometer. The procedures to measure formation and decay of $T201_{peroxo}$ were described previously (18). Second-order formation rate constants were obtained by plotting the pseudo-first-order formation rate constants versus the dioxygen concentrations used in the reactions and fit to a liner function to measure the slope (*SI Appendix*, Fig. S2).

ACKNOWLEDGMENTS. This work was supported by Grant GM032134 from the National Institute of General Medical Sciences (to S.J.L.) and a Camille and Henry Dreyfus Faculty Start-Up award (M.H.S.). Use of the Advanced Photon Source is supported by the US Department of Energy, Office of Basic Energy Sciences, under Contract DE-AC02-06CH11357. Portions of this research were carried out at the Stanford Synchrotron Radiation Laboratory, a national user facility operated by Stanford University on behalf of the US Department of Energy, Office of Basic Energy Sciences. The Stanford Synchrotron Radiation Lightsource Structural Molecular Biology Program is supported by the Department of Energy, Office of Biological and Environmental Research, and by the National Institutes of Health, National Center for Research Resources, Biomedical Technology Program, and the National Institute of General Medical Sciences.

1. Poulos TL, et al. (1985) The 26-Å crystal structure of Pseudomonas putida cytochrome P-450. *J Biol Chem* 260:16122–16130.
2. Stubbe J, Nocera DG, Yee CS, Chang MCY (2003) Radical initiation in the class I ribonucleotide reductase: Long-range proton-coupled electron transfer? *Chem Rev* 103:2167–2202.
3. Reece SY, Hodgkiss JM, Stubbe J, Nocera DG (2006) Proton-coupled electron transfer: The Mechanistic understanding for radical transport and catalysis in biology. *Philos Trans R Soc Lond B Biol Sci* 361:1351–1364.
4. Shih C, et al. (2008) Tryptophan-accelerated electron flow through proteins. *Science* 320:1760–1762.
5. Schoenborn BP, Watson HC, Kendrew JC (1965) Binding of xenon to sperm whale myoglobin. *Nature* 207:28–30.
6. Cohen J, et al. (2006) Finding gas diffusion pathways in proteins: Application to O_2 and H_2 transport in CpI [FeFe]-hydrogenase and the role of packing defects. *Structure* 13:1321–1329.
7. Montet Y, et al. (1997) Gas access to the active site of Ni-Fe hydrogenases probed by X-ray crystallography and molecular dynamics. *Nature* 4:523–526.
8. Doukov TI, et al. (2002) A Ni-Fe-Cu center in a bifunctional carbon monoxide dehydrogenase/acetyl-CoA synthase. *Science* 298:567–572.
9. Leahy JG, Batchelor PJ, Morcomb SM (2003) Evolution of the soluble diiron monooxygenases. *FEMS Microbiol Rev* 27:449–479.
10. Notomista E, Lahm A, Di Donato A, Tramontano A (2003) Evolution of bacterial and archaeal multicomponent monooxygenases. *J Mol Evol* 56:435–445.
11. Merkx M, et al. (2001) Dioxygen activation and methane hydroxylation by soluble methane monooxygenase: A tale of two irons and three proteins. *Angew Chem Int Ed Engl* 40:2782–2807.
12. Wallar BJ, Lipscomb JD (1996) Dioxygen activation by enzymes containing binuclear non-Heme iron clusters. *Chem Rev* 96:2625–2657.
13. Rosenzweig AC, Frederick CA, Lippard SJ, Nordlund P (1993) Crystal structure of a bacterial non-Haem iron hydroxylase that catalyses the biological oxidation of methane. *Nature* 366:537–543.
14. Whittington DA, Rosenzweig AC, Frederick CA, Lippard SJ (2001) Xenon and halogenated alkanes track putative substrate binding cavities in the soluble methane monooxygenase hydroxylase. *Biochemistry* 40:3476–3482.
15. McCormick MS (2004) Structural investigations of hydroxylase proteins and complexes in bacterial multicomponent monooxygenase systems. PhD Thesis (Massachusetts Inst of Technology, Cambridge, MA).
16. Sazinsky MH, Bard J, Di Donato A, Lippard SJ (2004) Crystal structure of the toluene/*o*-xylene monooxygenase hydroxylase from *Pseudomonas stutzeri* OX1. *J Biol Chem* 279:30600–30610.
17. Song WJ, et al. (2010) Active site threonine facilitates proton transfer during dioxygen activation at the diiron center of toluene/*o*-xylene monooxygenase hydroxylase. *J Am Chem Soc* 132:13582–13585.
18. Song WJ, et al. (2009) Characterization of a peroxodiiron(III) intermediate in the T201S variant of toluene/*o*-xylene monooxygenase hydroxylase from *Pseudomonas sp* OX1. *J Am Chem Soc* 131:6074–6075.
19. Liu Y, Nesheim JC, Lee S-K, Lipscomb JD (1995) Gating effects of component B on oxygen activation by the methane monooxygenase hydroxylase component. *J Biol Chem* 270:24662–24665.
20. Stahl SS, et al. (2001) Oxygen kinetic isotope effects in soluble methane monooxygenase. *J Biol Chem* 276:4549–4553.
21. Cafaro V, et al. (2002) Expression and purification of the recombinant subunits of toluene/*o*-xylene monooxygenase and reconstitution of the active complex. *Eur J Biochem* 269:5689–5699.
22. Pikus JD, et al. (1996) Recombinant toluene-4-monooxygenase: Catalytic and Mössbauer studies of the purified diiron and rieske components of a four-protein complex. *Biochemistry* 35:9106–9119.
23. Bailey LJ, McCoy JG, Phillips J, George N, Fox BG (2008) Structural consequences of effector protein complex formation in a diiron hydroxylase. *Proc Natl Acad Sci USA* 105:19194–19198.
24. Goto Y, Klinman JP (2002) Binding of dioxygen to non-metal sites in proteins: Exploration of the importance of binding site size versus hydrophobicity in the copper amine oxidase from *Hansenula polymorpha*. *Biochemistry* 41:13637–13643.
25. Al-Abdul-Wahid MS, Evanics F, Prosser RS (2011) Dioxygen transmembrane distributions and partitioning thermodynamics in lipid bilayers and micelles. *Biochemistry* 50:3975–3983.
26. Sazinsky MH, et al. (2006) X-ray structure of a hydroxylase-regulatory protein complex from a hydrocarbon-oxidizing multicomponent monooxygenase, *Pseudomonas sp.* OX1. *Biochemistry* 45:15392–15404.
27. Murray LJ, et al. (2007) Characterization of the arene-oxidizing intermediate in ToMOH as a diiron(III) species. *J Am Chem Soc* 129:14500–14510.
28. Murray LJ, et al. (2006) Dioxygen activation at non-Heme diiron centers: Characterization of intermediates in a mutant form of toluene/*o*-xylene monooxygenase hydroxylase. *J Am Chem Soc* 128:7458–7459.
29. Rosenzweig AC, et al. (1997) Crystal structure of the methane monooxygenase hydroxylase from *Methylococcus capsulatus* (Bath): Implications for substrate gating and component interactions. *Proteins* 29:141–152.
30. Murray LJ, et al. (2007) Dioxygen activation at non-Heme diiron centers: Oxidation of a proximal residue in the I100W variant of toluene/*o*-xylene monooxygenase hydroxylase. *Biochemistry* 46:14795–14809.
31. Song WJ, Lippard SJ (2011) Mechanistic studies of reactions of peroxodiiron(III) intermediates in T201 variants of toluene/*o*-xylene monooxygenase hydroxylase. *Biochemistry* 50:5391–5399.
32. DeLano WL (2002) *The PyMOL Molecular Graphics System* (DeLano Scientific, Palo Alto, CA) Version 1.4.
33. Xiong J, et al. (2000) The O_2 binding pocket of myohemerythrin: Role of a conserved leucine. *Biochemistry* 39:8526–8536.
34. Tomita A, et al. (2009) Visualizing breathing motion of internal cavities in concert with ligand migration in myoglobin. *Proc Natl Acad Sci USA* 106:2612–2616.
35. Gill SC, von Hippel PH (1989) Calculation of protein extinction coefficients from amino acid sequence data. *Anal Biochem* 182:319–326.
36. McCormick MS, Sazinsky MH, Condon KL, Lippard SJ (2006) X-ray crystal structures of manganese(II)-reconstituted and native toluene/o-xylene monooxygenase hydroxylase reveal rotamer shifts in conserved residues and an enhanced view of the protein interior. *J Am Chem Soc* 128:15108–15110.